

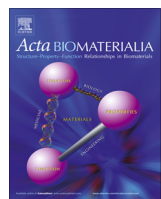


ELSEVIER

Contents lists available at ScienceDirect

Acta Biomaterialia

journal homepage: [www.elsevier.com/locate/actabiomat](http://www.elsevier.com/locate/actabiomat)



Full length article

## Dual pH-responsive multifunctional nanoparticles for targeted treatment of breast cancer by combining immunotherapy and chemotherapy



Yuanyuan Liu, Linan Qiao, Sipei Zhang, Guoyun Wan, Bowei Chen, Ping Zhou, Ning Zhang\*, Yinsong Wang\*

Tianjin Cancer Institute and Hospital, Laboratory of Breast Cancer Prevention and Therapy, Ministry of Education, Research Center of Basic Medical Science, School of Basic Medical Sciences, School of Pharmacy, Tianjin Key Laboratory on Technologies Enabling Development of Clinical Therapeutics and Diagnostics (Theranostics), Tianjin Medical University, Tianjin 300070, China

### ARTICLE INFO

#### Article history:

Received 19 June 2017

Received in revised form 13 October 2017

Accepted 7 November 2017

Available online 10 November 2017

#### Keywords:

Nanoparticle

Breast cancer

Targeting

Immunotherapy

Chemotherapy

### ABSTRACT

In the present study, a dual pH-responsive multifunctional nanoparticle system was designed for combining immunotherapy and chemotherapy to treat breast cancer through targeting immune cells and cancer cells. A proven anti-tumor immune regulator, R848, was encapsulated with poly(L-histidine) (PHIS) to form PHIS/R848 nanocores. Doxorubicin (DOX) was conjugated to hyaluronic acid (HA) through an acid-cleavable hydrazone bond linkage to synthesize polymeric prodrug HA-DOX, which was subsequently coated outside PHIS/R848 nanocores to form HA-DOX/PHIS/R848 nanoparticles. Ionization of PHIS around pH 6.5 (a pH value close to that of tumor microenvironment) switched the nature of this material from hydrophobic to hydrophilic, and thus triggered the release of R848 to exert immunoregulatory action. The rupture of hydrazone bond in HA-DOX at about pH 5.5 (pH of endo/lysosomes) accelerated the release of DOX to exert cytotoxic effects. In immune cells, PHIS/R848 nanocores exhibited strong immunoregulatory activities similar to those induced by free R848. In breast cancer cells overexpressing CD44, HA-DOX was specially internalized by CD44-mediated endocytosis and significantly inhibited the cell growth. In 4T1 tumor-bearing mice, HA-DOX/PHIS/R848 nanoparticles showed excellent tumor-targeting ability and remarkably inhibited the tumor growth by regulating tumor immunity and killing tumor cells. In summary, this multifunctional nanoparticle system could deliver R848 and DOX respectively to tumor microenvironment and breast cancer cells to achieve synergistic effects of immunotherapy and chemotherapy against breast cancer.

### Statement of Significance

Combination of immunotherapy and chemotherapy is becoming a promising new treatment for cancer. The major challenge is to target cancer and immune cells simultaneously and specifically. In this study, a dual pH-responsive multifunctional nanoparticle system based on poly(L-histidine) and hyaluronic acid was designed for co-loading R848 (immune-regulator) and doxorubicin (chemotherapeutic drug) through different encapsulation modes. By responding to the acidic pHs of tumor microenvironment and intracellular organelles, this multifunctional nanoparticle system could release R848 extracellularly and deliver DOX targetedly to breast cancer cells, thus achieving synergistic effects of immunotherapy and chemotherapy against breast cancer.

© 2017 Acta Materialia Inc. Published by Elsevier Ltd. All rights reserved.

### 1. Introduction

Breast cancer is the most common cancer and ranks the second-highest female mortality rate. In 2016, approximately 249,260 new breast cancer cases and 40,890 breast cancer deaths (40,450 women, 440 men) are estimated throughout the world [1]. Recent

\* Corresponding author.

E-mail addresses: [zhangning@tmu.edu.cn](mailto:zhangning@tmu.edu.cn) (N. Zhang), [wangyinsong@tmu.edu.cn](mailto:wangyinsong@tmu.edu.cn) (Y. Wang).

genetic studies have revealed that cancer is a highly heterogeneous disease where each tumor mass consists of cancer cells with different genetic backgrounds, which exhibit different malignancies and drug responsiveness [2]. Therefore, conventional chemotherapy with one single drug, although effective immediately, often result in deteriorated relapse in prolonged period of treatments. It has been proposed that blocking multiple targets simultaneously by combination therapy is an optimal strategy to combat cancer heterogeneity [3]. Some approaches have been tested in the laboratory and showed promising outcomes in clinical trials [4].

Nanotechnology, which allows delivery of multiple drugs in a controlled manner, shows unique advantages in combination therapy and needs further development. Different drugs can be co-loaded into a single nanocarrier system and co-delivered efficiently to the tumor through the enhanced permeability and retention (EPR) effect, and/or the active tumor-targeting effect; thus, this delivery mode is very favorable for exerting synergistic effects of these drugs [5,6]. Moreover, stimuli-sensitive or smart nanocarriers can effectively control drug release at the target site in a desirable fashion by responding to the inherent stimuli (e.g., pH, temperature, redox, enzymes, and reactive oxygen species) or the external stimuli (e.g., light, ultrasound, or magnetic field), thus alleviating toxic and side effects of the drugs on normal tissues [7]. To date, many tumor-targeted and stimuli-sensitive nanocarriers have been developed for targeted co-delivery and controlled release of antitumor drugs with different mechanisms, and some of them have shown significant synergistic effects [8,9].

Recent breakthroughs have revealed that immunotherapy is a new potent approach for cancer treatment [10,11]. Immunotherapy can modulate patient's own immunity to combat cancer, and therefore showing much lower toxicity and longer efficacy than the conventional treatment methods. Activation of dendritic cells (DCs), mediated by Toll-like receptors (TLR), plays a key role in anti-tumor immunity [12]. TLR agonists have been successfully employed to treat cancer in rodent tumor models [13,14]. Small-molecule agonists for Toll-like receptor (TLR) 7 and 8 have sparked a vivid interest in cancer research owing to their profound antitumor activity [15]. Resiquimod (R848) is a TLR7/8 agonist that can promote the maturation of DCs and enhance their functions through the myeloid differentiation factor (MyD88)-dependent pathway [16]. Compared to imiquimod, a TLR7/8 agonist approved by the US Food and Drug Administration (FDA) for topical administration in cancer therapy [14], R848 can induce more pronounced cytokine secretion and macrophage activation. Combination of immunotherapy with chemotherapy shows promising outcomes for patients, and recently, some carrier systems have been developed for co-delivery of immunotherapeutic and chemotherapeutic drugs. A thermosensitive hydrogel system based on poly(ethylene glycol)-poly( $\gamma$ -ethyl-L-glutamate) diblock copolymers was prepared for co-delivery of interleukin-15 and cisplatin, and significant synergistic effects were achieved against melanoma [17]. Lim et al. designed a stable dispersion system containing both paclitaxel and imiquimod using poly ( $\gamma$ -glutamic acid) as the matrix. In DCs, this dispersion system remarkably enhanced the secretion of pro-inflammatory and Th1 cytokines [18]. However, none of these co-delivery systems addressed the differentiated targeting of immune cells versus tumor cells.

In the present study, a dual pH-responsive multifunctional nanoparticle system based on poly(L-histidine) (PHIS) and hyaluronic acid (HA) was designed for combining immunotherapy and chemotherapy to treat breast cancer through targeting immune cells and cancer cells simultaneously and specifically. PHIS is a peptide containing branched imidazole group that has lone pairs of electrons on the unsaturated nitrogen, which endows

this peptide with pH-dependent amphoteric property [19]. The ionization of PHIS at around pH 6.5, a pH value close to that of tumor microenvironment [20], can switch the nature of this material from hydrophobic to hydrophilic [21]. HA is an acidic polysaccharide that consists of alternating units of  $\beta$ -1,4-D-glucuronic acid- $\beta$ -1,3-N-acetyl-D-glucosamine [22,23]. As a natural ligand for CD44 that is often overexpressed by breast cancer cells, HA has been widely used in active targeting treatment of breast cancer [24–26]. The preparation of this multifunctional nanoparticle system is illustrated in Scheme 1A. R848-loaded PHIS (PHIS/R848) nanocores are first prepared in a weak alkaline solution. DOX is conjugated to HA through an acid-cleavable hydrazone bond linkage to synthesize polymeric prodrug HA-DOX. Next, HA-DOX is coated outside PHIS/R848 nanocores to form HA-DOX/PHIS/R848 nanoparticles, thus realize the co-loading of R848 and DOX. Scheme 1B illustrates the function mechanisms of HA-DOX/PHIS/R848 nanoparticles. After intravenous injection, HA-DOX/PHIS/R848 nanoparticles are delivered to and accumulated in the tumor site through the EPR and active targeting effects. In weakly acidic tumor microenvironment, the hydrophobic/hydrophilic transformation of PHIS triggers the disintegration of HA-DOX/PHIS/R848 nanoparticles, which further mediates the release of R848 to exert its activation effects targeting immune cells. On the other hand, HA-DOX is specifically internalized into breast cancer cells through CD44-mediated endocytosis and the rupture of the hydrazone bond then occurs in response to the acidic endo/lysosomal pH. Hence, DOX is released in breast cancer cells to exert its cytotoxic effects. In this study, we also investigated the *in vitro* and *in vivo* effects of this multifunctional nanoparticle system to evaluate its potential for combination treatment on breast cancer.

## 2. Materials and methods

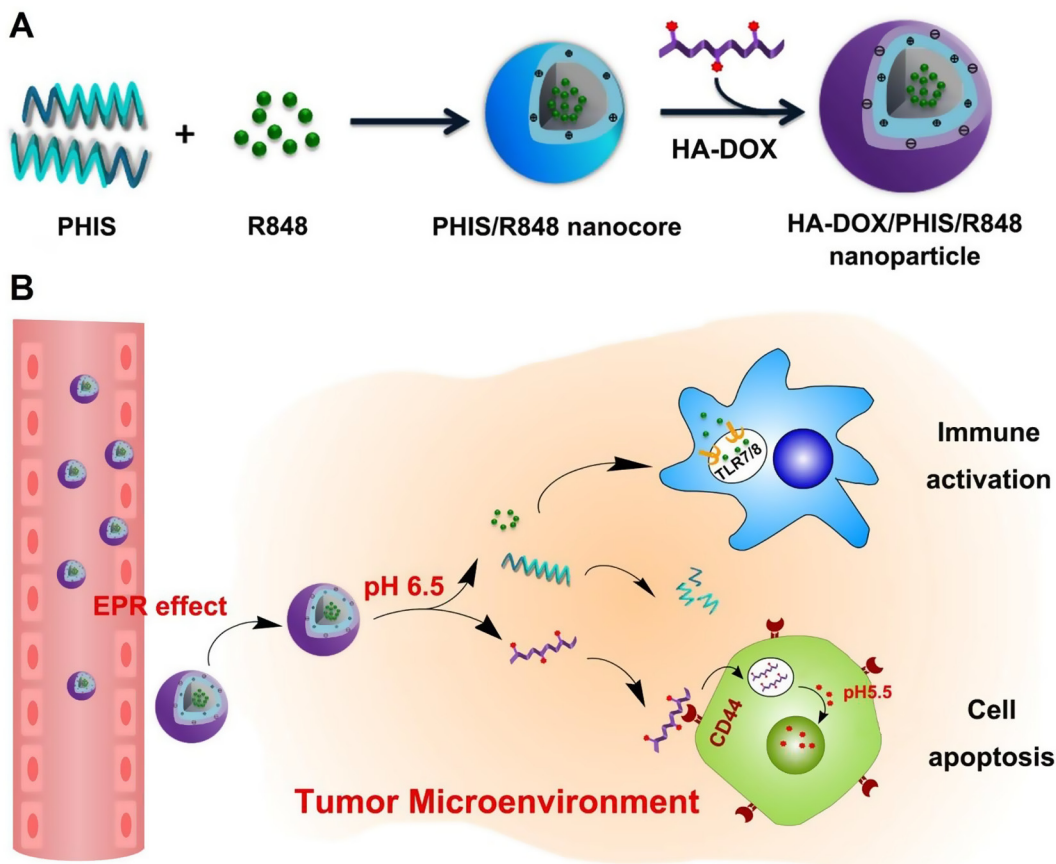
### 2.1. Materials

HA with molecular mass of 47 kDa was purchased from Bloomage Freda Biopharm (Jinan, China). DOX-HCl was obtained from Meilun Biology Technology (Dalian, China). Succinic dihydrazide, D-Luciferin, 1-(3-Dimethylaminopropyl)-3-ethylcarbodiimide hydrochloride (EDC), N-hydroxysuccinimide (NHS), 3,3'-dioctade cyloxacarbocyanine perchlorate (Dio), and 4',6-diamidino-2-phenylindole (DAPI) were purchased from Sigma-Aldrich (St. Louis, USA). Cyanine 5.5 (Cy5.5) was obtained from Fanbo BioChemicals (Beijing, China). Cell counting kit-8 (CCK-8) was purchased from Dojindo (Japan). All other chemical reagents were analytical grade and obtained from various commercial sources.

### 2.2. Cells and animals

Human breast cancer cell lines (MCF-7 and MDA-MB-231) and mouse breast cancer cell lines (4T1 and luciferase-labeled 4T1 (4T1-Luc)) were obtained from American Type Culture Collection (ATCC) and cultured in DMEM medium (Gibco, Life Technologies, USA) containing 10% v/v fetal bovine serum (FBS) and 1% v/v penicillin/streptomycin. Dendritic cell (DC) lines including murine DC2.4 and human DC-like CAL-1 were gifted by Dr. De Yang from Frederick National Laboratory for Cancer Research (Frederick, Maryland, USA). Murine macrophage RAW264.7 cell line was obtained from ATCC. These cells were cultured in RPMI 1640 medium (Invitrogen, Carlsbad, CA) supplemented with 10% (v/v) FBS.

Sprague-Dawley rats and female Balb/c normal and nude mice were bought from the Laboratory Animal Center (Tianjin Medical University, China) and housed in a specific pathogen-free environ-



**Scheme 1.** Schematic illustrations for the preparation of HA-DOX/PHIS/R848 nanoparticles (A) and their functional mechanisms in breast cancer treatment (B).

ment. All animal experiments were carried out according to the protocols approved by the Tianjin Medical University Animal Care and Use Committee.

### 2.3. Synthesis and characterization of HA-DOX

HA-DOX was synthesized according to a method previously reported [27]. HA was first reacted with succinic dihydrazide to synthesize HA-SDH. Briefly, 50 mg of HA was dissolved in deionized water and activated by reaction with 8 mg of EDC and 5 mg of NHS for 30 min. Next, 20 mg of succinic dihydrazide was added and the pH of the mixture was adjusted to be approximately 4.8. After stirring at room temperature for 24 h, the mixture was transferred into a dialysis bag (Millipore, molecular weight cut off 8–14 kDa, USA) and dialyzed against water. Finally, the dialyzed solution was lyophilized to obtain HA-SDH.

DOX was next conjugated to HA-SDH through an acid-cleavable hydrazone bond. A total of 100 mg of HA-SDH was dissolved in 20 mL of 2 mM phosphate buffer saline (PBS) solution with pH 6.5, and 12 mg of DOX was then added under stirring. The pH of the mixture was adjusted to be approximately 6.5, and the reaction was allowed to continue for 24 h. Subsequently, the mixture was dialyzed against 2 mM PBS solution with pH 7.4, and the dialyzed solution was then lyophilized to obtain the red, cotton wool-like product of HA-DOX. The chemical structures of HA and HA-DOX were confirmed by infrared (IR) spectroscopy and proton nuclear magnetic resonance (<sup>1</sup>H NMR) spectra on a NEXUS 470 IR spectrometer (Nicolet, USA) and a AVANCE III NMR spectrometer (400 MHz, Bruker, Germany), respectively. The weight content of DOX in HA-DOX was determined by an ultraviolet-visible (UV/Vis) spectrophotometer (U-3310, Hitachi, Japan) at 488 nm.

### 2.4. Preparation and characterization of HA-DOX/PHIS/R848 nanoparticles

First, PHIS/R848 nanocores were prepared by a nanoprecipitation method at PHIS/R848 weight ratios of 10/1, 10/2, 10/3, 10/4, and 10/5. Briefly, a certain amount of R848 and 10 mg PHIS were dissolved in 500 μL of methanol and the mixture was then added dropwise to 5 mL borax buffer with pH 8.8 to obtain a slightly milky solution. This solution was stirred at 800 rpm for 2 h at room temperature to remove methanol and then sonicated in an ice bath to obtain PHIS/R848 nanocores. The unloaded R848 was removed by ultrafiltration. Ultra performance liquid chromatography (UPLC) method was used to detect the amount of R848 in PHIS/R848 nanocores on an ACQUITY UPLC system (ACQ-BSM, Waters). C18 analytical column (50 mm × 2.1 mm, 1.7 μm, Waters) was used and column temperature was set at 37 °C. The mobile phase consisted of methanol/0.05 M KH<sub>2</sub>PO<sub>4</sub>/triethylamine (55/45/0.2, v/v/v, pH 3.0), and the flow rate was 0.2 mL/min. The injection volume was 2 μL. The detection wavelength was set at 246 nm. The loading content and encapsulation efficiency of R848 were calculated according to the following formulas.

$$\text{Loading content} = (\text{mass of loaded R848}/\text{mass of nanoparticles}) \times 100\%$$

$$\text{Encapsulation efficiency} = (\text{mass of loaded R848}/\text{total mass of fed R848}) \times 100\%$$

Next, HA-DOX was coated outside PHIS/R848 nanocores by incubation in aqueous media (pH 7.4) under stirring for 2 h to prepare HA-DOX/PHIS/R848 nanoparticles. The weight ratios of HA-

DOX to PHIS/R848 nanocores were separately set at 1/4, 1/2, 1/1, and 2/1. The uncoated HA-DOX was removed using an ultrafiltration method through a 300-kDa cut-off filter (Millipore, USA). For the following cell and animal experiments, we also prepared HA-DOX/PHIS/Dio and HA-DOX/PHIS/Cy5.5 nanoparticles by the same method, in which R848 was replaced with Dio (a green fluorescent membrane dye) or Cy5.5 (a hydrophilic near-infrared dye) during the preparation of PHIS nanocores.

The sizes, size distributions, and zeta potentials of PHIS/R848 nanocores and HA-DOX/PHIS/R848 nanoparticles were measured by an automatic particle analyzer (Zetasizer Nano ZS, Malvern, UK) at sample concentrations of approximately 0.5 mg/mL. Their morphologies were also observed by a transmission electron microscope (TEM, Hitachi HT7700, Tokyo, Japan). In addition, the *in vitro* stabilities of PHIS/R848 nanocores and HA-DOX/PHIS/R848 nanoparticles were evaluated by monitoring their size change after storage in 10% calf serum for different times.

## 2.5. Drug release studies

The *in vitro* release of DOX and R848 from HA-DOX/PHIS/R848 nanoparticles was measured in PBS solutions at pH 7.4, 6.5, and 5.5 using a dynamic dialysis method. A total of 5 mg of nanoparticle samples were dispersed in 50 mL release media and then placed in an air bath at  $37 \pm 0.2$  °C under shaking at 100 rpm. At designated time intervals, 0.5 mL of release media was removed and 0.5 mL of fresh release media was added. The amount of released R848 was detected using the UPLC method. The amount of released DOX was measured by the UV/Vis spectrophotometric method.

## 2.6. Evaluation of maturation of DC2.4 cells induced by PHIS/R848 nanocores

Maturation of DC2.4 cells induced by PHIS/R848 nanocores was evaluated by detecting the protein expression of CD80, CD83 and CD86 using an immunofluorescence method. PHIS/R848 nanocores were first processed by incubation in culture media at pH 6.5 for 6 h. Then, DC2.4 cells were seeded in 6-well plates and treated with free R848 or processed PHIS/R848 nanocores for 24 h at R848 concentration of 5 µg/mL. Subsequently, the cells were collected and fixed in 4% paraformaldehyde for 15 min at room temperature. Next, the cells were resuspended in fluorescence-activated cell sorting buffer and stained with FITC-conjugated antibodies against CD80, CD83, and CD86 (eBioscience, San Diego, CA, USA) at 4 °C for 30 min. After washing with PBS solution 2 times, the cells were finally analyzed using a flow cytometer (BD Pharmingen, San Diego, CA, USA). In addition, the effects of blank material PHIS on DC2.4 cells were also measured using the same method at PHIS concentration of 25 µg/mL.

## 2.7. Assessment of activation of CAL-1 cells stimulated by PHIS/R848 nanocores

Activation of CAL-1 cells stimulated by PHIS/R848 nanocores was assessed by determining the cellular mRNA expression of proinflammatory cytokines, including interferon- $\alpha$  (IFN- $\alpha$ ), tumor necrosis factor- $\alpha$  (TNF- $\alpha$ ), interleukin-6 (IL-6), and IL-12p40 by real-time quantitative polymerase chain reaction (qTR-PCR). PHIS/R848 nanocores were first processed by incubation in culture media at pH 6.5 for 6 h. Subsequently, CAL-1 cells were treated with free R848 or processed PHIS/R848 nanocores at different drug concentrations for 8 h. Next, the total RNA was extracted from the cells using Trizol® Reagent (Life Technologies, USA). One microgram of RNA was reverse transcribed into cDNA with a RT kit (Roche, Basel, Switzerland) and then assayed by FastStart Universal

SYBR Green Master (Rox) (Roche) based qRT-PCR on 7500 Fast Real Time PCR System (Applied Biosystems, USA) using glyceraldehyde-3-phosphate dehydrogenase (GAPDH) as the housekeeping gene. The data were presented as mRNA accumulation index ( $2^{-\Delta\Delta Ct}$ ). The primer sequences used were as follows: IFN- $\alpha$  (sense: 5'-TTA GGC TCA CCC ATT TCA ACC-3', antisense: 5'-CAC AGA GCA GCT TGA CTT GC-3'); TNF- $\alpha$  (sense: 5'-GGC AAC CAC TAA GAA TTC AAA-3', antisense: 5'-TCT CCA GAT TCC AGA TGT CAG-3'); IL-6 (sense: 5'-AAA TTC GGT ACA TCC TCG ACG G-3', antisense: 5'-GGA AGG TTC AGG TTG TTT TCT GC-3'); IL-12p40 (sense: 5'-ACA AAG GAG GCG AGG TTC TAA-3', antisense: 5'-CCC TTG GGG GTC AGA AGA G-3'); GAPDH (sense: 5'-TGC ACC ACC AAC TGC TTA GC-3', antisense: 5'-GGC ATG GAC TGT GGT CAT GAG-3'). In addition, the effects of blank material PHIS on CAL-1 cells were also measured using the same method at different concentrations.

## 2.8. Analysis of CD44 expression in MCF-7, 4T1, MDA-MB-231, DC2.4, and RAW264.7 cells by flow cytometry

We determined the expression levels of CD44 in breast cancer cells (MCF-7, 4T1, and MDA-MB-231) and immune cells (DC2.4 and RAW264.7) by flow cytometry. Briefly, the cells were suspended in staining buffer (PBS with 1% FBS, 2 mM EDTA, and 0.1% sodium azide) and incubated with the PE-conjugated IgG specific for CD44 (Biolegend, USA) at 4 °C for 30 min. Appropriate PE-irrelevant isotype controls (Biolegend, USA) were used at the same protein concentration as the test antibody. After washing with ice-cold staining buffer, the cells were fixed with 1% formaldehyde and then examined by a flow cytometer (Beckman Coulter, USA).

## 2.9. Analysis of cellular uptakes and intracellular locations of HA-DOX and HA-DOX/PHIS/Dio nanoparticles

The uptakes of HA-DOX in MCF-7 and DC2.4 cells after incubation for different time periods were detected by flow cytometry. Briefly, MCF-7 and DC2.4 cells were seeded into 6-well culture plates and then incubated with HA-DOX at DOX concentration of 2 µg/mL. At predetermined fixed times, the cells were detached with 0.125% trypsin, resuspended in PBS solution containing 0.1% bovine serum albumin, and finally analyzed by a flow cytometer. The intracellular locations of HA-DOX in MCF-7 and DC2.4 cells were observed using confocal microscopy. The cells were seeded in the confocal dishes at a density of  $1 \times 10^4$  cells/well for 24 h, and free DOX or HA-DOX was then added at concentration of 2 µg/mL DOX. After incubation for different time periods, the cells were washed with PBS solution thrice and stained with DAPI. Finally, the cells were observed using a confocal microscope (FV-1000, Olympus, Japan).

Moreover, the intracellular location of HA-DOX/PHIS/Dio nanoparticles in MCF-7 cells was also observed to evaluate the pH-responsive drug release property. Briefly, free Dio or HA-DOX/PHIS/Dio nanoparticles were first processed in culture media at pH 7.4 or 6.5, respectively, for 6 or 12 h. MCF-7 cells were then incubated with the above free Dio and HA-DOX/PHIS/Dio nanoparticles at the same Dio concentrations for an additional 12 h. Next, the cells were fixed with 4% paraformaldehyde and stained with DAPI. Finally, the intracellular locations of green and red fluorescence signals from Dio and DOX, respectively, were observed by a confocal microscope.

## 2.10. Cell viability assay

The CCK-8 assay was used to evaluate cytotoxicities of HA-DOX, PHIS/R848 nanocores, and HA-DOX/PHIS/R848 nanoparticles in MCF-7, 4T1, RAW264.7, and DC2.4 cells, and free R848 and free

DOX were used as the controls. Briefly, the cells were seeded into 96-well plates with a density of  $5 \times 10^3$  cells/well and cultured for 24 h. The culture media were then replaced with the fresh culture media containing free R848, free DOX, HA-DOX, PHIS/R848 nanocores, and HA-DOX/PHIS/R848 nanoparticles at different drug concentrations. After further incubation for 24 or 48 h, the cells were processed with CCK reagent, and the absorbance was then measured at 450 nm using an ELX800 absorbance microplate reader (Bio-tek EPOCH, Winooski, VT, USA).

### 2.11. In vivo pharmacokinetic characteristic of HA-DOX

Sprague-Dawley rats were grouped into two groups with 6 mice per group and intravenously injected with free DOX and HA-DOX at a dose of 6 mg/kg DOX. Approximately 200 mL of blood samples was collected at predefined time intervals. The samples were centrifuged for 10 min at 13,000 rpm, and the supernatants were then extracted with ethyl acetate. The ethyl acetate extract was then volatilized by nitrogen at 40 °C, and the residue was dissolved in 200 mL mobile phase. Finally, the plasma concentrations of DOX were detected by the UPLC method as previously reported [28].

### 2.12. Biodistributions of HA-DOX and HA-DOX/PHIS/R848 nanoparticles

Breast cancer xenograft mouse model was constructed by transplanting 4T1 cells subcutaneously to the nude mice and used in the following experiments at 10 d after inoculation. First, we evaluated the tissue distributions of HA-DOX. 4T1 tumor-bearing mice were separately intravenously injected with free DOX and HA-DOX at a dose of 8.0 mg/kg DOX. At 8 or 24 h post injection, these mice were sacrificed, and the tumors and major organs including the heart, liver, spleen, lung, and kidney were collected for imaging by an IVIS in vivo imaging system (PerkinElmer, Waltham, USA). Next, we evaluated the tumor-targeted delivery ability of HA-DOX/PHIS/Cy5.5 nanoparticles. Briefly, 4T1 tumor-bearing mice were injected with normal saline (control), free Cy5.5, PHIS/Cy5.5 nanocores, and HA-DOX/PHIS/Cy5.5 nanoparticles through the tail vein, and then imaged using an in vivo imaging system at 2, 6 and 24 h post administration. The tumors and main organs were then removed from these mice for further fluorescence imaging.

### 2.13. Evaluation of in vivo antitumor efficacy of HA-DOX/PHIS/R848 nanoparticles

For evaluation of in vivo antitumor efficacy, two orthotopic breast cancer models were established by implanting 4T1 and 4T1-Luc cells separately into the mammary fat pad of female Balb/c mice. When the 4T1 tumors reached 100 mm<sup>3</sup> in size, the mice were randomly grouped into five groups with 6 mice per group and respectively received treatments of normal saline (control), free DOX, free R848, DOX/R848 mixture, and HA-DOX/PHIS/R848 nanoparticles. All treatments were administered by intravenous injection once every 2 d for 4 consecutive times. Treatment doses of DOX and R848 were 2 and 3.5 mg/kg, respectively. Tumor volumes were measured every 2 d. At 22 d after the first administration, all mice were sacrificed, and the main organs and tumors were then excised for the following histopathological and immunohistochemical examinations. Moreover, 4T1-Luc tumor-bearing mice were given the same treatments with 2 mice per group. At the end of treatments, the mice were intraperitoneally injected with D-Luciferin, and their lungs were then removed for further bioluminescence imaging.

For histopathological examination, the excised organs and tumors were fixed in 4% paraformaldehyde, embedded in paraffin, and sectioned into 5-μm-thick slices. The sections were then

stained with hematoxylin and eosin (H&E, Sigma-Aldrich, St. Louis, USA) and then imaged with a fluorescence microscope (IX71, Olympus, Japan). For detecting CD3<sup>+</sup> and CD8<sup>+</sup> T cells in tumor tissues, immunohistochemical stainings were performed on tumor sections by using primary antibodies against CD3 and CD8 (Abcam, Cambridge, MA) at 1:100 dilution at 4 °C overnight. The sections were then processed with secondary antibody of goat anti-rabbit IgG and HRP-linked antibody (Zsbio, China). Finally, the stained sections were observed under a fluorescence microscope.

### 2.14. Statistical analysis

All tests were carried out independently at least three times, and the data are presented as mean ± standard deviation. Statistical analysis was performed using Student's *t*-test, and *p* < .05 was considered as statistically significant.

## 3. Results and discussion

### 3.1. Preparation, characterization, and drug loading capability of HA-DOX/PHIS/R848 nanoparticles

In this study, we designed a multifunctional nanoparticle system composed of hydrophobic PHIS/R848 nanocores and hydrophilic HA-DOX shells for targeted treatment of breast cancer by combining immunotherapy with chemotherapy. PHIS has pH-responsive hydrophobic/hydrophilic transformation property, and many investigations have used it to develop pH-sensitive nanomicelle and nanoparticle carriers [19–21]. Here, we first prepared PHIS/R848 nanocores with different PHIS/R848 weight ratios in borax buffer (pH 8.8) by using the nanoprecipitation method. During the preparation, the hydrophobic interaction was a main driving force for loading R848 into nanocores. As shown in Table S1, PHIS/R848 nanocores had gradually increased size and widened size distribution with the increase in PHIS/R848 weight ratio, but their zeta potentials remained relatively constant. Considering the application essentials, e.g., small size, narrow size dispersion, and high drug loading capacity, a ratio of 10:3 was believed as an optimal PHIS/R848 weight ratio and used in the subsequent experiments. PHIS/R848 nanocores had a regular spherical shape (Fig. 1A) and a small size of approximately 153.1 nm with a polydispersity index of 0.128 (Fig. 1B). Their zeta potential was approximately 33.8 mV, indicating their highly positive charged surfaces. The loading content and encapsulation efficiency of R848 in PHIS/R848 nanocores were 22.8% and 76%, respectively.

Next, HA-DOX was synthesized by two-step reactions according to the method previously reported [27]. As shown in Fig. S1A, HA-SDH was first synthesized through the reaction of HA with succinic dihydrazide under the activation of EDC/NHS and DOX was then conjugated to HA-SDH through an acid-cleavable hydrazone linkage to obtain HA-DOX. The chemical structure of HA-DOX was confirmed by the IR and <sup>1</sup>H NMR techniques. In the IR spectrum of HA-DOX (Fig. S1B), the characteristic stretching vibration of the carbonyl group in DOX appeared at around 1731 cm<sup>-1</sup>. In the <sup>1</sup>H NMR spectrum of HA-DOX (Fig. S1C), the characteristic peaks of anthracene protons in DOX and alkyl protons in succinic dihydrazide were clearly observed at 7.3–7.6 ppm and 2.4–2.7 ppm, respectively. These results were consistent with those reported previously [19,29]. The content of DOX in HA-DOX was determined by the UV/Vis method, and its value was approximately 6.5%. Because of the presence of a large number of negative charges, HA-DOX could efficiently coat outside positively charged PHIS/R848 nanocores through ionic interaction to form HA-DOX/PHIS/R848 nanoparticles. Here, we prepared HA-DOX/PHIS/R848 nanoparticles at different weight ratios of HA-DOX to PHIS/R848

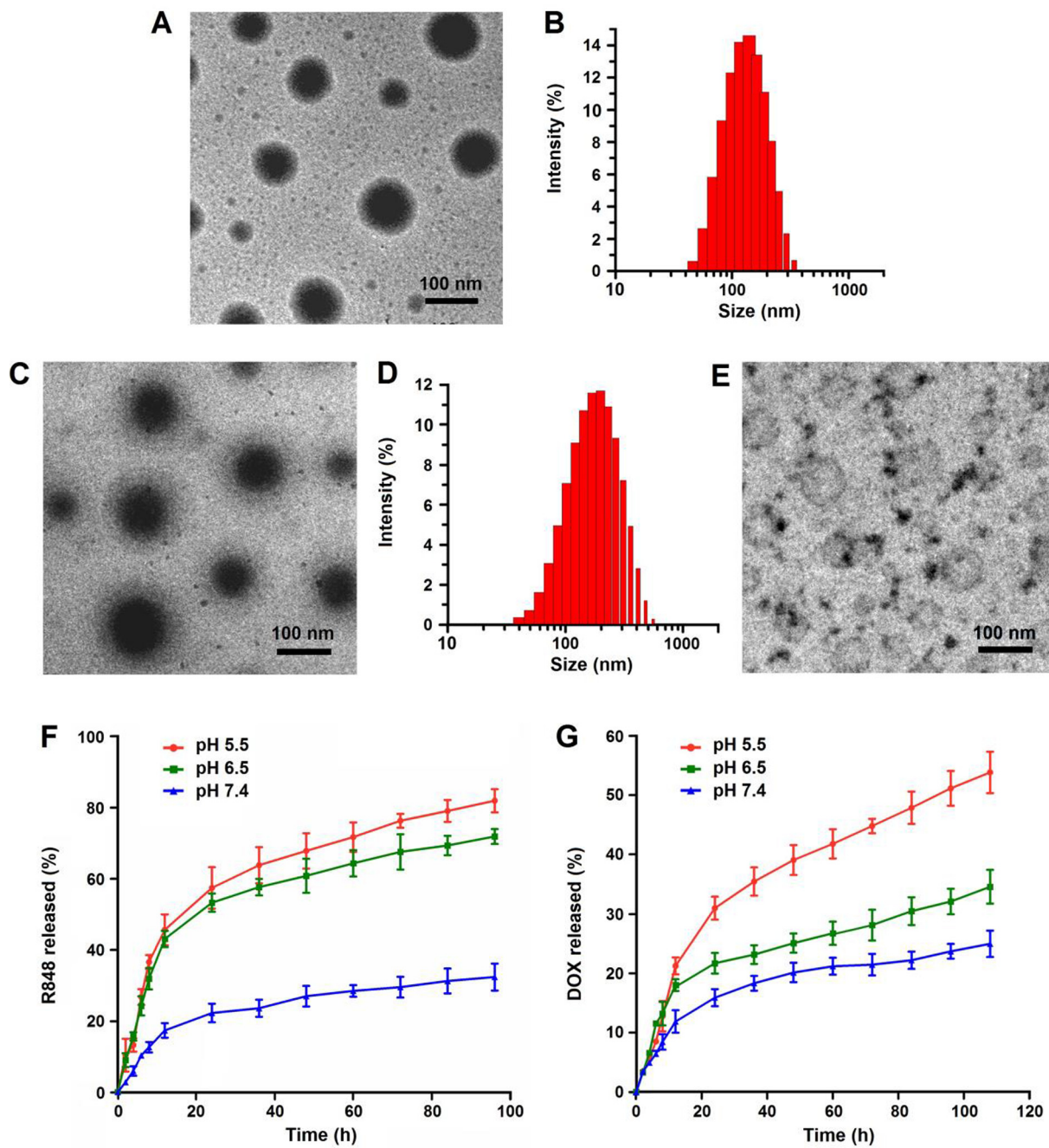


**Fig. 1.** Morphological characterization and *in vitro* drug release of HA-DOX/PHIS/R848 nanoparticles. TEM images of PHIS/R848 nanocores (A) and HA-DOX/PHIS/R848 nanoparticles (C) in weak alkaline aqueous media. The size distributions of PHIS/R848 nanocores (B) and HA-DOX/PHIS/R848 nanoparticles (D). The TEM image of HA-DOX/PHIS/R848 nanoparticles in weak acidic aqueous medium (E). The *in vitro* release of R848 (F) and DOX (G) from HA-DOX/PHIS/R848 nanoparticles at different pHs.

nanocores and characterized these nanoparticles. As shown in Table S2, HA-DOX/PHIS/R848 nanoparticles had larger sizes, and their zeta potentials changed from positive to negative as compared to PHIS/R848 nanocores. This suggested that HA-DOX was successfully coated outside PHIS/R848 nanocores. When the weight ratio was 2:1, HA-DOX/PHIS/R848 nanoparticles exhibited a good *in vitro* stability and their size almost did not change during storage in 10% calf serum for 9 d (Table S3); thus, they were used in the subsequent experiments. The TEM image showed that HA-DOX/PHIS/R848 nanoparticles had a classic “core-shell” structure (Fig. 1C), and their size was approximately 200 nm with a polydispersity index of 0.215 (Fig. 1D). The weight ratio of R848 to DOX loaded in these nanoparticles was about 1.75.

### 3.2. pH-responsive drug release properties of HA-DOX/PHIS/R848 nanoparticles

In the previous investigation, Bae and his coworkers reported that PHIS had pH-dependent amphoteric property because of the presence of rich imidazole groups in its molecule and produced a maximum response of hydrophobic-to-hydrophilic switch at pH 6.5 [30], which occurred in the pH range (6.2–6.9) of tumor microenvironment [20]. We believed that this pH-responsive switch could induce the disintegration of HA-DOX/PHIS/R848 nanoparticles and further trigger the rapid release of R848. To confirm this, we observed the morphological changes of HA-DOX/PHIS/R848 nanoparticles after storage at pH 6.5 for 6 h and evalu-

ated the *in vitro* release of R848 at different pHs. As shown in Fig. 1E, HA-DOX/PHIS/R848 nanoparticles were obviously disintegrated, and the debris of PHIS/R848 nanocores was almost completely removed from HA-DOX shells. Fig. 1F shows that the *in vitro* release of R848 from HA-DOX/PHIS/R848 nanoparticles at pH 6.5 and 5.5 was significantly faster than that at pH 7.4, but there was no significant difference between the release of R848 at pH 6.5 and pH 5.5. These results demonstrated that the disintegration of HA-DOX/PHIS/R848 nanoparticles mediated the release of R848 at the acidic pHs, which further suggested that R848 could be efficiently released in tumor microenvironment. DOX also exhibited significant pH-responsive *in vitro* release from HA-DOX/PHIS/R848 nanoparticles, but its release rate was much higher at pH 5.5 than at pH 6.5 and pH 7.4 (Fig. 1G). This was because the rupture of the hydrazone bond in HA-DOX occurred rapidly at pH 5.5; this finding was consistent with previous reports [29,31]. In view of acidic conditions within endo/lysosomes (pH 5.0–6.0) [32], we deduced that DOX might be released from HA-DOX in endo/lysosomes to exert its antitumor effects after cellular internalization by CD44-mediated endocytosis.

To further evaluate the abovementioned pH-responsive drug release properties, we prepared HA-DOX/PHIS/Dio nanoparticles, in which R848 was replaced by Dio (a green fluorescence dye for lipophilic membrane), and then observed subcellular locations of fluorescence signals from Dio and DOX in MCF-7 cells after incubation with HA-DOX/PHIS/Dio nanoparticles pre-processed at pH 7.4 or 6.5. The confocal images are shown in Fig. 2. Free Dio was mainly located in the cell membrane, and its green fluorescence was very weak in the cytoplasm. In contrast, the green fluorescence of Dio from HA-DOX/PHIS/Dio nanoparticles that were pre-

processed at pH 7.4 either for 6 or 12 h was almost wholly located in the cytoplasm, indicating that Dio entered MCF-7 cells through cellular internalization of HA-DOX/PHIS/Dio nanoparticles. However, in MCF-7 cells treated with HA-DOX/PHIS/Dio nanoparticles that were pre-processed at pH 6.5 for 6 h, Dio was not only located in the cytoplasm but also in the cell membrane, suggesting that Dio had been partially released from nanoparticles during the period of pre-processing. Furthermore, with the pre-processing time extending to 12 h at pH 6.5, the green fluorescence of Dio was only observed in the cell membrane, indicating that Dio had been mostly released from HA-DOX/PHIS/Dio nanoparticles. From the above results, we deduced that R848 could be efficiently released from HA-DOX/PHIS/R848 nanoparticles in tumor microenvironment. Further, the DOX fluorescence was mainly located in the cell nuclei, and the fluorescence intensities in all treatment groups showed no significant difference. This suggested that HA-DOX successfully entered MCF-7 cells and DOX was then efficiently released through the rupture of the hydrazone bond in response to endo/lysosomal pHs.

### 3.3. Immunoregulatory activities of PHIS/R848 nanocores in immune cells

DCs are potent antigen-presenting cells that link innate and adaptive immune responses. Once activated through triggering of their pattern recognition receptors such as TLRs, they acquire a mature state and migrate to the lymph nodes where they can activate T cells and direct the immune responses that can subsequently attack and destroy the tumor cells [13]. R848 is a TLR7/8 agonist that can promote the maturation of DCs and enhance their

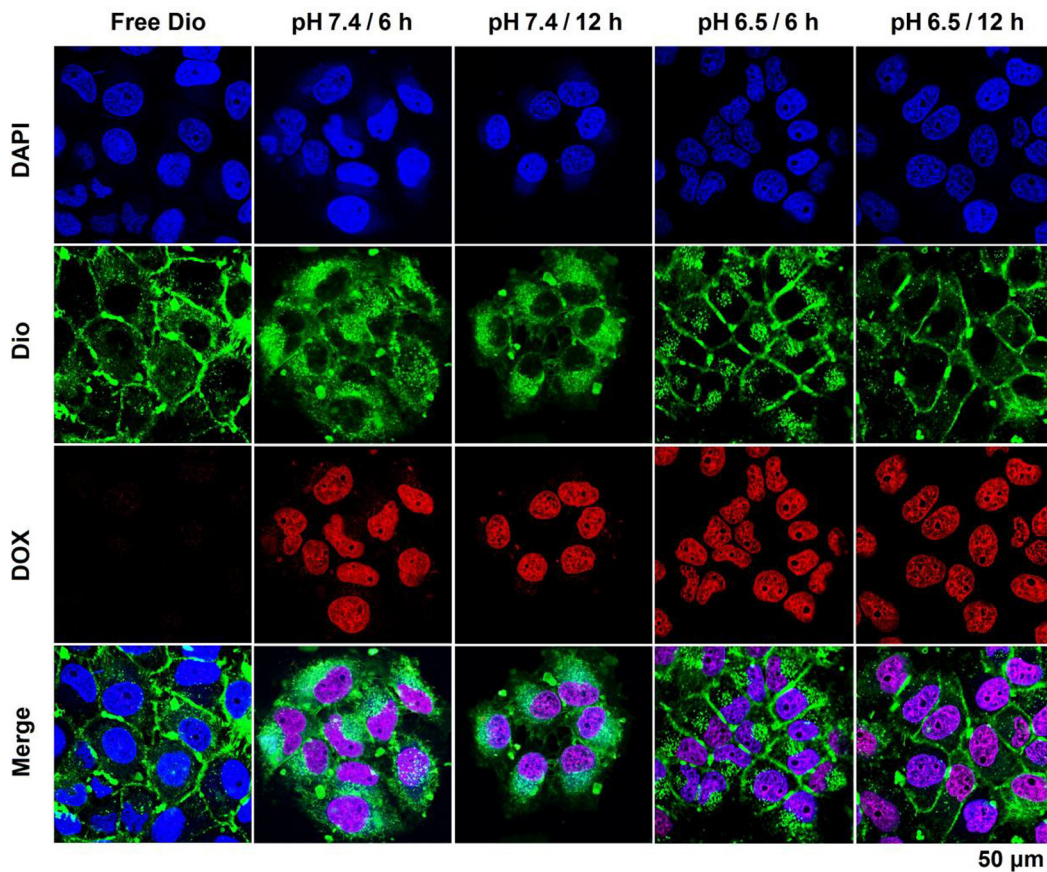


**Fig. 2.** The confocal images of MCF-7 cells after incubations with free Dio and HA-DOX/PHIS/Dio nanoparticles. The nanoparticles were pre-processed for 6 or 12 h at pH 7.4 and 6.5, respectively.

functions through the myeloid differentiation factor (MyD88)-dependent pathway [16]. Matured DCs often express high levels of surface molecular markers such as CD80, CD86, and CD83, in which CD80/CD86 is known as co-stimulatory molecules for the activation of helper T cells [33]. Therefore, we evaluated the immunoregulatory activities of PHIS/R848 nanocores by detecting the protein expression of CD80, CD86, and CD83 in murine DC2.4 cells by using the immunofluorescence method. As shown in Fig. 3A, B and C, CD80, CD86 and CD83 were significantly upregulated in DC2.4 cells after treatment with free R848 and PHIS/R848 nanocores as compared to the control. Furthermore, there were no significant differences in the expression levels of these markers between the two treatment groups; this finding demonstrates that PHIS/R848 nanocores had effects similar to those of free R848 on maturation and activation of DCs.

CAL-1 cells share many phenotypic and functional properties of human plasmacytoid DCs, e.g., they also express TLRs (TLR7 and TLR9) and can recognize CpG motif-containing oligonucleotides [34,35]. Upon activation through the TLRs/MyD88 signaling pathway, CAL-1 cells can produce large amounts of type I IFNs and some proinflammatory cytokines [36]. Thus, we further assessed the immunoregulatory activities of PHIS/R848 nanocores in CAL-1 cells by detecting the mRNA levels of IFN- $\alpha$  (a known type I IFN) and some proinflammatory cytokines including IL-6, TNF- $\alpha$  and IL-12p40 in CAL-1 cells by using the qTR-PCR technique. As shown respectively in Fig. 3D and E, free R848 and PHIS/R848 nanocores both upregulated the mRNA expression of proinflammatory cytokines in a concentration-dependent manner. In free R848 treatment, the mRNA expression levels of IFN- $\alpha$ , IL-6, TNF- $\alpha$ , and IL-12p40 reached their peaks at R848 concentration range of 0.5–1.0  $\mu$ g/mL. However, in the treatment of PHIS/R848 nanocores, the mRNA expression peaks of these proinflammatory cytokines appeared at 1–5  $\mu$ g/mL R848. Furthermore, the peak value of IFN- $\alpha$  mRNA induced by PHIS/R848 nanocores was obviously higher than that induced by free R848, but the peak levels of other proinflammatory cytokines in the two treatment groups were consistent. Blank material PHIS did not exhibit significant effects on the activation of DC2.4 cells (Fig. S2A) and CAL-1 cells (Fig. S2B). All the above mentioned results indicated that PHIS/R848 nanocores could activate DCs to produce type I IFNs and some proinflammatory cytokines identical to that done by free R848.

In addition, we investigated the influence of PHIS/R848 nanocores on the proliferation of DC2.4 cells and murine RAW264.7 macrophages by the CCK-8 assay. As shown in Fig. S3A and S3B, free R848 and PHIS/R848 nanocores remarkably improved the proliferation of DC2.4 and RAW264.7 cells, especially for RAW264.7 cells, which displayed strong proliferative activity even at a very low R848 concentration. However, both free R848 and PHIS/R848 nanocores did not affect the growth of breast cancer MCF-7 cells (Fig. S3C) and 4T1 cells (Fig. S3D) at the same R848 concentrations. These results suggested that PHIS/R848 nanocores exerted selective effects on immune cells.

#### 3.4. CD44-mediated cellular internalization of HA-DOX in breast cancer cells

Considering that HA is a natural ligand for CD44, a cell-surface adhesion receptor that is often overexpressed in cancer cells and cancer stem cells, many investigations have used HA to develop carrier systems for targeted delivery of anticancer drugs, and some of them have shown potential clinical applications [24,37]. Two strategies are often used for designing HA-based carrier systems. The first one is to prepare polymeric prodrug by conjugation of anticancer drugs to HA and the second one is to use HA as a targeting material for surface modification of nanoparticles containing anticancer drugs. In this study, we synthesized HA-DOX conjugate

through the hydrazone bond and hoped to realize selective effects of DOX on breast cancer cells through the specific and high affinity of HA for CD44. To verify this selectivity, we first detected the expression levels of CD44 on breast cancer cells (MCF-7, 4T1, and MDA-MB-231) and immune cells (DC2.4 and RAW264.7) by the immunofluorescence technique. The flow cytometric data are shown in Fig. 4. MCF-7, 4T1, and MDA-MB-231 cells exhibited very high expression levels of CD44 (Fig. 4A), whereas DC2.4 and RAW264.7 cells expressed CD44 at far lower levels (Fig. 4B). This suggested that HA-DOX could exert selective effects on breast cancer cells as compared to immune cells.

Next, we detected cellular internalizations and intracellular locations of HA-DOX in MCF-7 cells (high CD44 expression) and DC2.4 cells (low CD44 expression) to evaluate the selectivity of HA-DOX for breast cancer cells. The confocal images of MCF-7 and DC2.4 cells after incubation with HA-DOX are shown respectively in Fig. 4C and E. In both types of cells, the fluorescence signals from DOX were enhanced as time progressed and gradually translocated from the cytoplasm to the cell nuclei. This suggested that DOX was efficiently released from HA-DOX through the rupture of the hydrazone bond in endo/lysosomes after cellular internalization. By contrast, the fluorescence signals were much stronger in MCF-7 cells than that in DC2.4 cells during the 12-h incubation period. In addition, we also detected the uptakes of HA-DOX in MCF-7 and DC2.4 cells by flow cytometry. HA-DOX displayed much stronger fluorescence intensities and faster cell entry speed in MCF-7 cells (Fig. 4D) than in DC2.4 cells (Fig. 4F). From above results, it could be deduced that CD44-mediated cellular internalization was the main cell entry mechanism for HA-DOX. Thus, we deduced that HA-DOX could exert antitumor effects selectively in breast cancer cells with high expressions of CD44.

#### 3.5. *In vitro* cytotoxicities of HA-DOX and HA-DOX/PHIS/R848 nanoparticles in breast cancer cells and immune cells

We assessed the *in vitro* cytotoxicities of HA-DOX and HA-DOX/PHIS/R848 nanoparticles in breast cancer cells and immune cells using the CCK8 assay. In breast cancer MCF-7 and 4T1 cells, free DOX, HA-DOX and HA-DOX/PHIS/R848 nanoparticles showed time- and concentration-dependent cytotoxicities. Compared to free DOX, HA-DOX and HA-DOX/PHIS/R848 nanoparticles had evidently lower cytotoxicities (Fig. S4A and S4B), e.g., the IC<sub>50</sub> value of free DOX in 4T1 cells was approximately 0.17  $\mu$ g/mL, whereas the IC<sub>50</sub> values of HA-DOX and HA-DOX/PHIS/R848 nanoparticles were up to 0.47 and 0.64  $\mu$ g/mL DOX, respectively. When the treatment time extended to 48 h, the cytotoxicities of HA-DOX and HA-DOX/PHIS/R848 nanoparticles in MCF-7 and 4T1 cells were obviously increased much faster than that of free DOX (Fig. 5A and B), e.g., the IC<sub>50</sub> value of free DOX was approximately 0.08  $\mu$ g/mL in 4T1 cells, whereas the IC<sub>50</sub> values of HA-DOX and HA-DOX/PHIS/R848 nanoparticles decreased respectively to 0.13 and 0.18  $\mu$ g/mL. This was because HA-DOX and HA-DOX/PHIS/R848 nanoparticles could fully exert their cytotoxic effects only when DOX was completely released in breast cancer cells. In addition, free R848 and PHIS/R848 nanocores exhibited no significant toxicities in breast cancer cells (Fig. S3C and S3D) due to the lack of direct antitumor effects of R848 as discussed before.

In DC2.4 and RAW264.7 cells, the cytotoxicities of HA-DOX were very significantly lower than that of free DOX at both 24 h (Fig. S4C and S4D) and 48 h (Fig. 5C and D) after treatment. For example, the IC<sub>50</sub> values of free DOX at 48 h were only approximately 0.09 and 0.05  $\mu$ g/mL in DC2.4 and RAW264.7 cells, respectively, but the IC<sub>50</sub> values of HA-DOX were high at 0.56 and 0.35  $\mu$ g/mL DOX. This was because HA-DOX could not be fully taken up by immune cells through the CD44-mediated cell entry pathway due to the relatively low expression levels of CD44 by these cells.

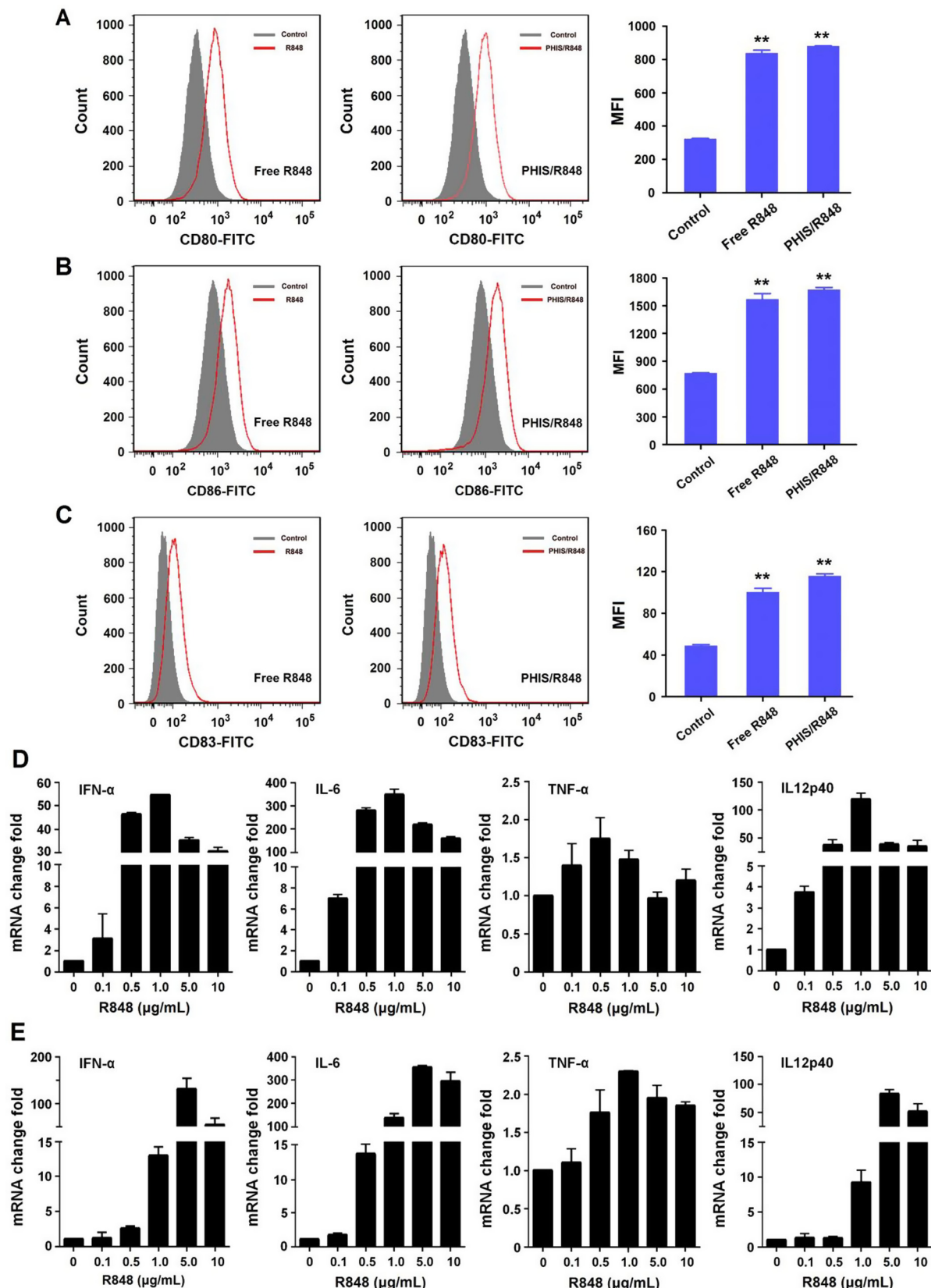


**Fig. 3.** PHIS/R848 nanocores promoted the maturation and activation of DCs. The protein expression levels of CD80 (A), CD86 (B), and CD83 (C) in DC2.4 cells with treatments of free R848 and PHIS/R848 nanocores at the R848 concentration of 5 µg/mL. The mRNA expression levels of IFN- $\alpha$ , IL-6, TNF- $\alpha$ , and IL-12p40 in CAL-1 cells treated with free R848 (D) and PHIS/R848 nanocores (E) at different R848 concentrations. All data are represented as mean  $\pm$  SD from at least 3 separate experiments. \*\* indicates  $P < .01$  compared to the control.

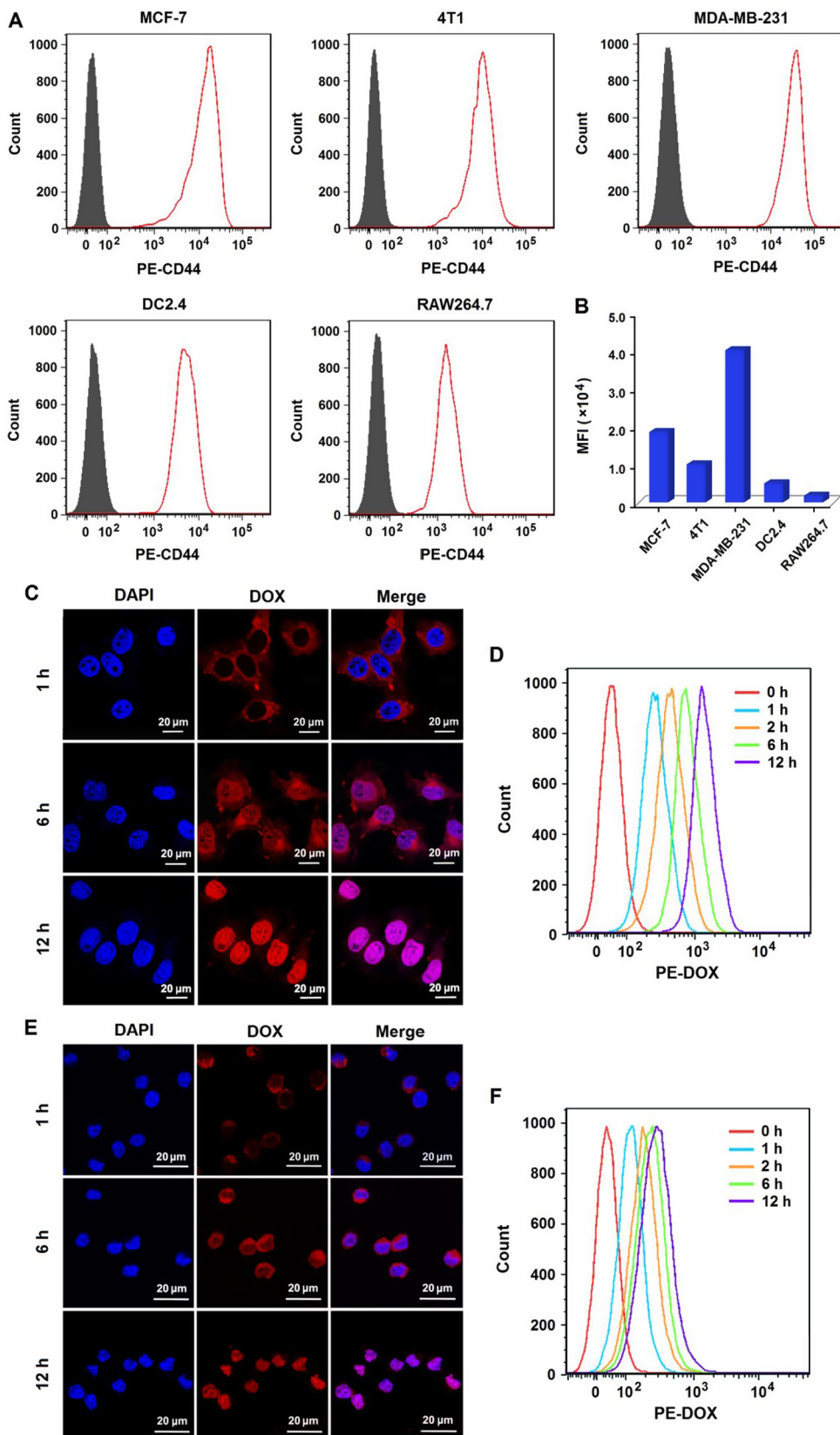


**Fig. 4.** Selective internalization of HA-DOX in breast cancer cells by the CD44-mediated endocytosis. (A) The flow cytometric analysis of CD44 expressed by MCF-7, 4T1, MDA-MB-231, DC2.4, and RAW264.7 cells. (B) The CD44 expression levels in these cells. The confocal images of MCF-7 (C) and DC2.4 cells (E) after incubation with HA-DOX for 1, 6, and 12 h. The flow cytometric profiles of MCF-7 (D) and DC2.4 cells (F) after incubation with HA-DOX for 0, 1, 2, 6, and 12 h. The DOX concentration was approximately 2  $\mu$ g/mL.

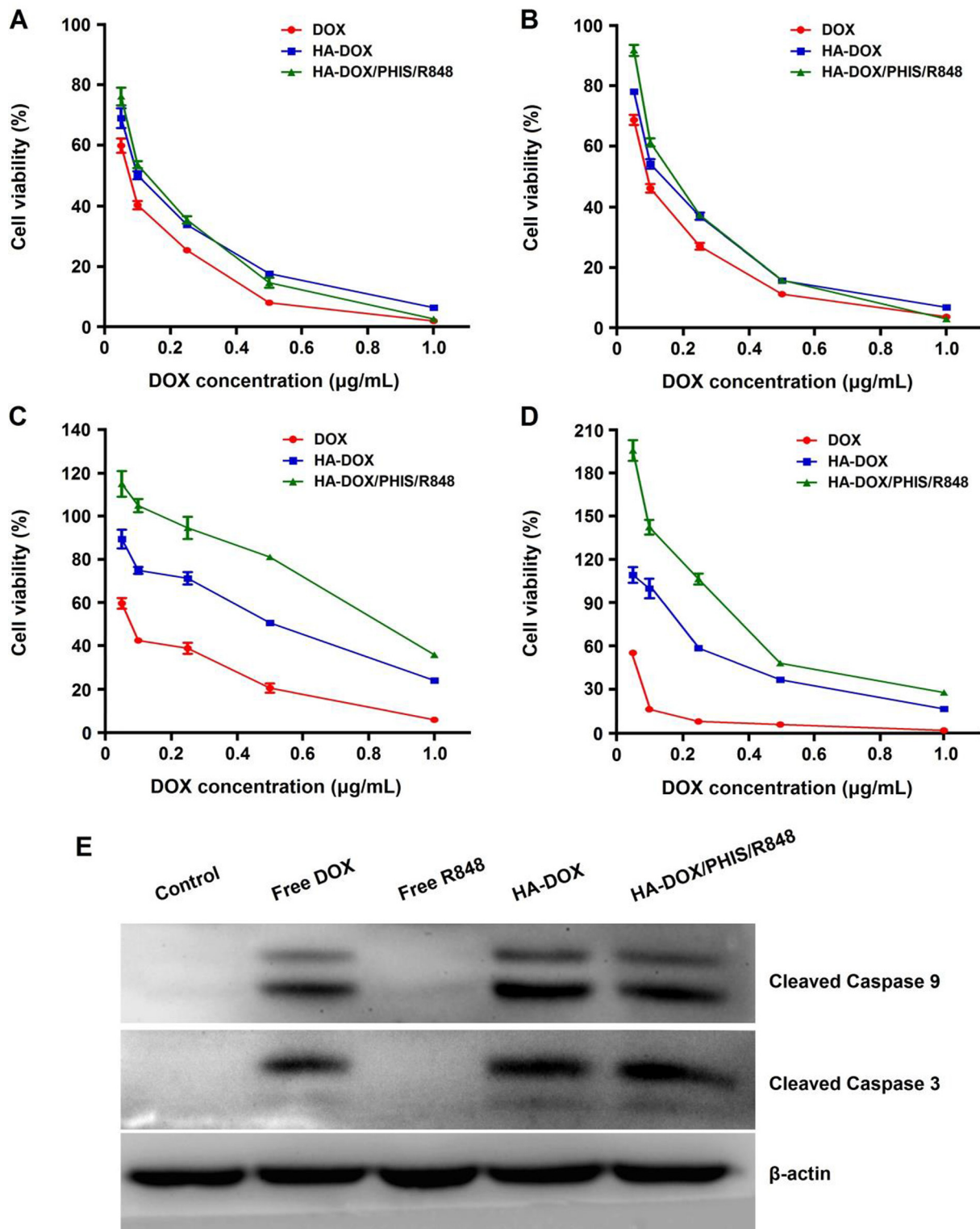


**Fig. 5.** *In vitro* cytotoxicities of HA-DOX/PHIS/R848 nanoparticles in breast cancer cells and immune cells. The cytotoxicities of free DOX, HA-DOX, and HA-DOX/PHIS/R848 nanoparticles in MCF-7 (A), 4T1 (B), DC2.4 (C), and RAW264.7 cells (D) determined by the CCK8 assay. The expression levels of cleaved Caspase-9 and Caspase-3 in MCF-7 cells detected by the western blotting technique (E). The weight ratio of R848 to DOX in HA-DOX/PHIS/R848 nanoparticles was approximately 1.75.

Compared to HA-DOX, HA-DOX/PHIS/R848 nanoparticles exhibited significantly reduced cytotoxicities in DC2.4 and RAW264.7 cells, and even promoted the proliferation of these cells within a certain range of DOX concentrations (Fig. 5C and D) due to the regulatory effects of R848. From the above results, we deduced that HA-DOX/PHIS/R848 nanoparticles possessed the combined therapeutic

effects on breast cancer by directly killing cancer cells and indirectly modulating the activity and proliferation of immune cells.

Considering that the activation of caspase cascades is the main mechanism in DOX-induced cell apoptosis, we further measured the expression levels of cleaved Caspase-9 and Caspase-3 (activated forms) in MCF-7 cells after different treatments by using

the western blotting technique. The results are shown in Fig. 5E. Compared to the control, HA-DOX and HA-DOX/PHIS/R848 nanoparticles greatly promoted the expression levels of cleaved Caspase-9 and Caspase-3, which were even slightly higher than that induced by free DOX. This finding indicated that HA-DOX/PHIS/R848 nanoparticles could directly kill breast cancer cells by inducing cell apoptosis. However, PHIS/R848 nanocores did not induce the apparent expression of cleaved Caspase-9 and Caspase-3 in MCF-7 cells, suggesting their nondirect therapeutic effects on breast cancer cells.

### 3.6. Tissue distribution and tumor accumulation of HA-DOX/PHIS/Cy5.5 nanoparticles in 4T1 tumor-bearing mice

To evaluate the ability of the nanoparticle system targeting breast cancer, we further prepared HA-DOX/PHIS/Cy5.5 nanoparticles, in which Cy5.5 was used to replace R848, and then detected

their tissue distribution and tumor accumulation in 4T1 tumor-bearing mice. The fluorescence images of mice at 2, 6, and 24 h after intravenous injections of normal saline (control), free Cy5.5, PHIS/Cy5.5 nanocores, and HA-DOX/PHIS/Cy5.5 nanoparticles are shown in Fig. 6A. Free Cy5.5 was mainly distributed in the bladder at 2 h after injection and almost completely excreted from the body of mouse at 24 h. This indicated that free Cy5.5 had a rapid elimination rate in 4T1 tumor-bearing mice. Further, free Cy5.5 did not display apparent distribution in the tumor. In contrast, PHIS/Cy5.5 nanocores and HA-DOX/PHIS/Cy5.5 nanoparticles showed obvious tumor distribution at 6 h and were almost distributed only in the tumors at 24 h, thus indicating their good tumor targeting abilities through the EPR effect. Next, major organs (heart, liver, kidney, spleen, and lung) and tumors were excised for further imaging. As shown in Fig. 6B, HA-DOX/PHIS/Cy5.5 nanoparticles exhibited enhanced tumor accumulations and reduced liver distributions as compared to PHIS/Cy5.5 nanocores. This suggested

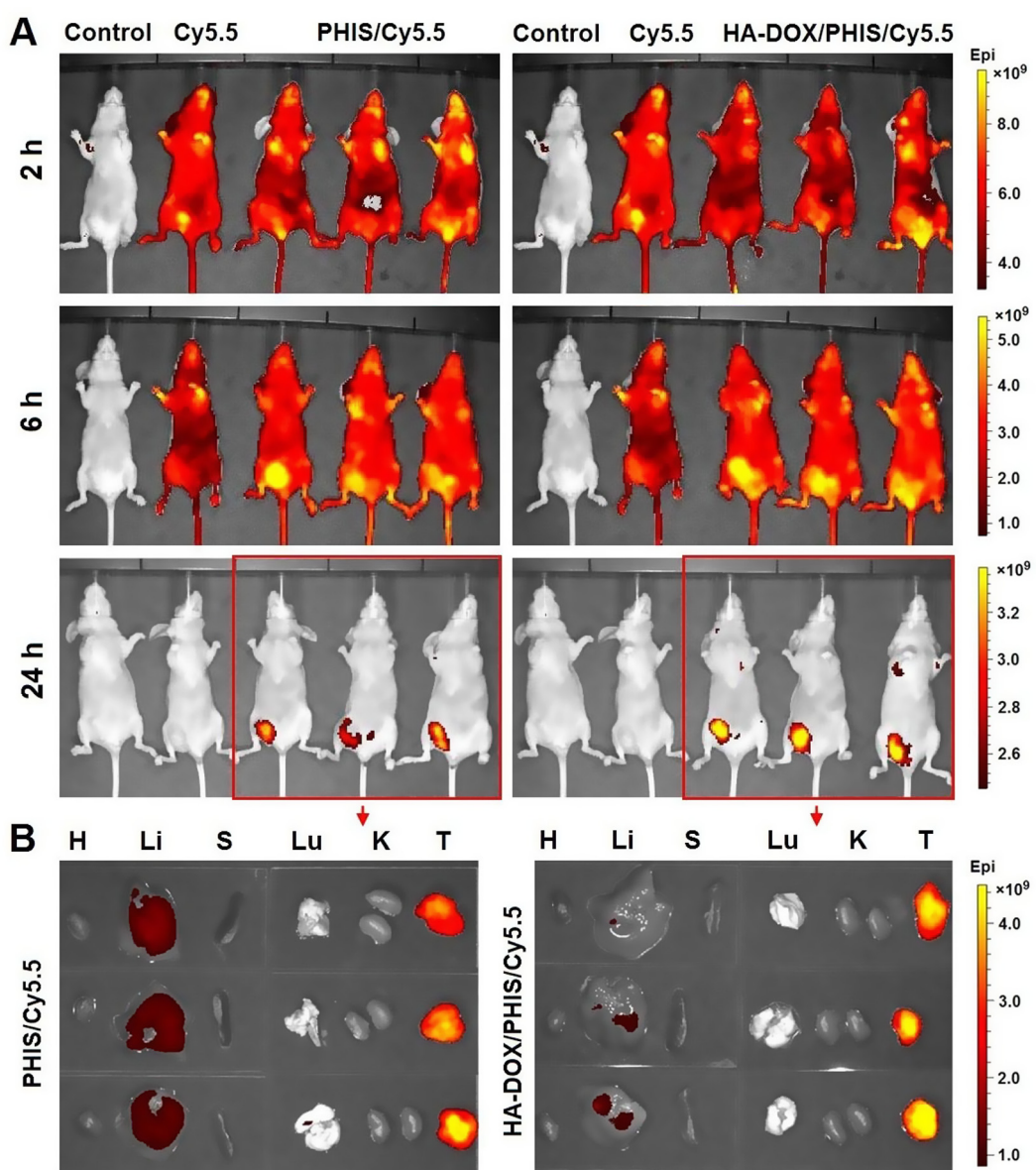


**Fig. 6.** Tissue distributions and tumor accumulations of PHIS/Cy5.5 nanocores and HA-DOX/PHIS/Cy5.5 nanoparticles in 4T1 cells tumor-bearing mice. (A) The in vivo fluorescence images of mice at 2, 6 and 24 h after intravenous injections of normal saline (the control), free Cy5.5, PHIS/Cy5.5 nanocores, and HA-DOX/PHIS/Cy5.5 nanoparticles at the same Cy5.5 doses. (B) The fluorescence images of the major organs including the heart (H), liver (Li), spleen (S), lung (L), kidney (K), and tumors (T) removed from mice with different treatments.

that the active targeting effect of HA-DOX improved the tumor accumulation of HA-DOX/PHIS/Cy5.5 nanoparticles.

Moreover, we also evaluated the *in vivo* pharmacokinetic characteristics and tissue distributions of free DOX and HA-DOX. The pharmacokinetic profiles are shown in Fig. S5A. Clearly, HA-DOX

significantly prolonged the blood circulation time of DOX in rats. For free DOX, the  $t_{1/2}$  value was only 3.07 h, but the  $t_{1/2}$  value of HA-DOX was high at 21.03 h. These results confirmed that HA-DOX had a good stability *in vivo*. The fluorescence images of main tissues and tumors in 4T1 tumor-bearing mice at 8 and 24 h after

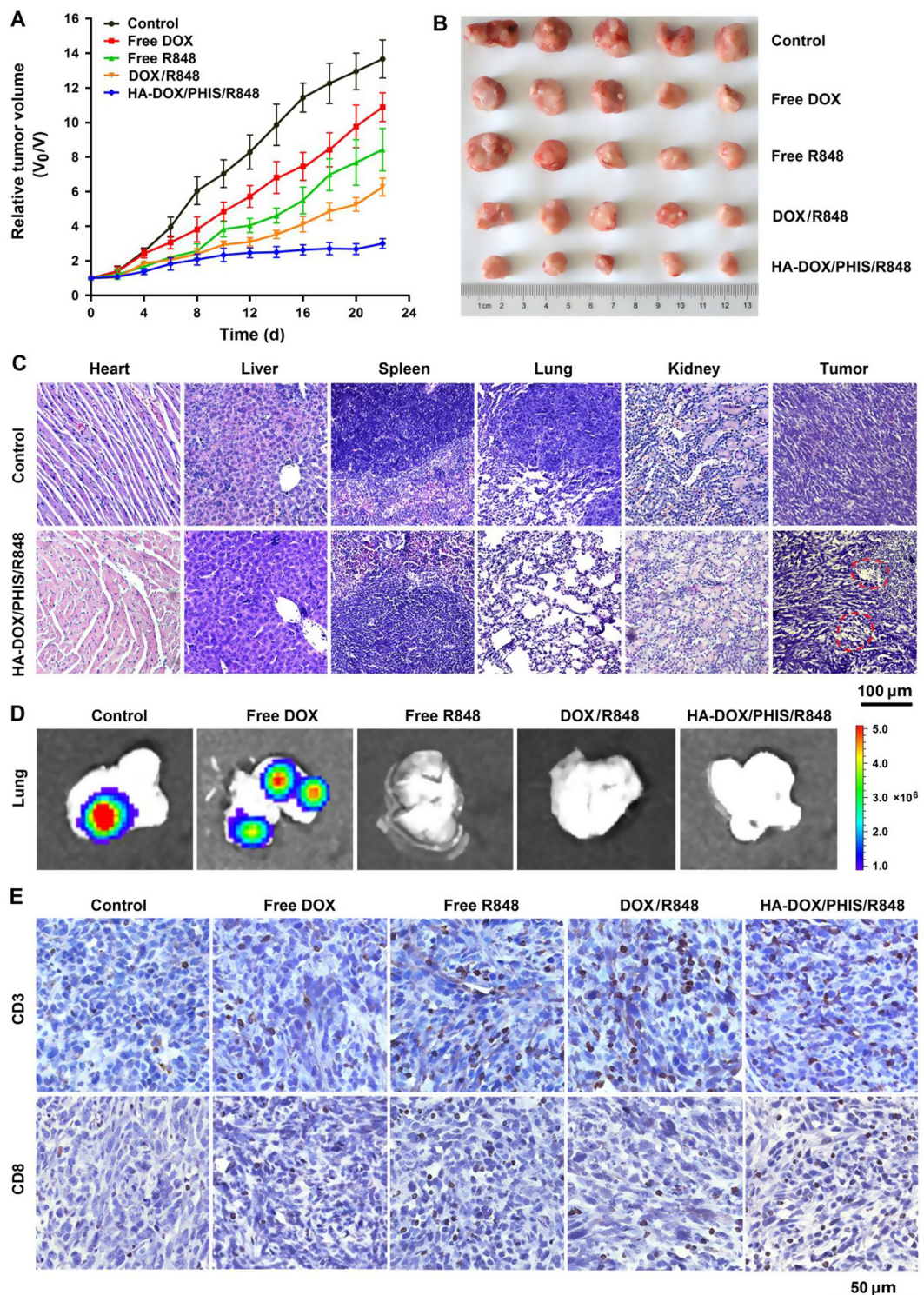


**Fig. 7.** Antitumor efficacy of HA-DOX/PHIS/R848 nanoparticles in 4T1 tumor-bearing mice. (A) The curves of tumor growth in mice with treatments of normal saline (control), free DOX, free R848, DOX/R848 mixture, and HA-DOX/PHIS/R848 nanoparticles. (B) The image of tumors removed from mice with different treatments. (C) The images of H&E-stained sections from the main organs and tumors in the control and HA-DOX/PHIS/R848 nanoparticles treatment groups. The necrotic areas are marked by the red dotted lines. (D) The bioluminescence images of lungs removed from 4T1-Luc tumor-bearing mice after various treatments and injection of d-Luciferin. (E) The immunohistochemical images of tumor sections stained with anti-CD3 and anti-CD8 antibodies. Brown color represents positive staining of CD3<sup>+</sup> or CD8<sup>+</sup> T cells. All data are represented as mean  $\pm$  SD ( $n = 6$ ).

administration are shown in Fig. S5B and S5C, respectively. Compared to free DOX, HA-DOX remarkably increased the tumor distributions of DOX, suggesting that HA-DOX possessed distinct breast cancer targeting capacity through its specific affinity for CD44. From all the above results, it could be deduced that the prolonged circulation effect and active targeting ability of HA-DOX played important roles in the in vivo targeted delivery of HA-DOX/PHIS/Cy5.5 nanoparticles.

### 3.7. Antitumor efficacy of HA-DOX/PHIS/R848 nanoparticles in 4T1 tumor-bearing mice

The antitumor efficacy of HA-DOX/PHIS/R848 nanoparticles was estimated in 4T1 tumor-bearing mice. All treatments including free DOX, free R848, DOX/R848 mixture, and HA-DOX/PHIS/R848 nanoparticles were administered through intravenous injection every 2 d for 4 consecutive times. During the treatment period, the changes in tumor volumes were detected continuously for 22 d, and the main organs and tumors were removed for further histopathological and immunohistochemical examinations. The curves of tumor growth are shown in Fig. 7A. Compared to the control group, free DOX slightly inhibited the growth of 4T1 tumors in mice at dose of 2 mg/kg, which was consistent with the results previously reported wherein low-dose DOX treatment could not efficiently suppress the growth and progression of breast cancer [38,39]. However, DOX/R848 mixture significantly inhibited the tumor growth compared to both free DOX and free R848, demonstrating the synergistic effects of these two drugs on breast cancer by combining immunotherapy and chemotherapy. More importantly, HA-DOX/PHIS/R848 nanoparticles showed significantly enhanced tumor-inhibitory activity in contrast to DOX/R848 mixture. As shown in Fig. 7B, the tumors in the treatment group of HA-DOX/PHIS/R848 nanoparticles were much smaller than those in the other treatment groups. We believed that the strong antitumor efficacy of HA-DOX/PHIS/R848 nanoparticles was because R848 and DOX could be efficiently delivered to the tumor site and then released successively in tumor microenvironment and tumor cells to exert their synergistic effects.

The images of H&E-stained tissue and tumor sections are displayed in Figs. 7C and S6. Compared to the control mice, no pathological changes were detected in the heart, liver, spleen and kidney, but the necrosis phenomenon was evidently observed in the tumors in 4T1 tumor-bearing mice treated with HA-DOX/PHIS/R848 nanoparticles. Lung metastasis appeared in the control mice, but was almost unseen in the mice treated with HA-DOX/PHIS/R848 nanoparticles (Fig. 7C). As previously reported, lung metastasis usually occurred at 2 or 3 weeks after 4T1 tumor inoculation due to the high metastatic potential of 4T1 cell line [40]; thus, we believed that HA-DOX/PHIS/R848 nanoparticles could effectively suppress the lung metastasis of breast cancer. In addition, the lung metastasis was also observed in the image of H&E-stained lung section in the treatment group of free DOX (Fig. S4). Next, we established 4T1-Luc breast cancer mouse model to assess the inhibitory effect of HA-DOX/PHIS/R848 nanoparticles on breast cancer metastasis by using the bioluminescence imaging technique. As shown in Fig. 7D, the lung metastasis in 4T1-Luc tumor-bearing mouse was nearly completely prevented by treatment of free R848, DOX/R848 mixture and HA-DOX/PHIS/R848 nanoparticles as compared to both the control and free DOX-treated mice. This suggested that R848 played a major role in suppressing breast cancer metastasis, which was consistent with previous investigations [41,42].

T cells are among the most versatile cells in the body and play a central role in adaptive immunity. CD3 is a useful immunohistochemical marker for the detection of T cells in tissue sections due to its high specificity and presence at all stages of T cell devel-

opment. In the thymus, T cells are matured through a stepwise process and undergo positive and negative selection to produce CD4<sup>+</sup> and CD8<sup>+</sup> T cells. CD8<sup>+</sup> T cells are also called cytotoxic T lymphocytes. Once activated, they can induce the death of cancer cells, cells that are infected particularly with viruses, or cells that are damaged in other ways [43]. Some studies have found that TLR7/8 agonists such as imiquimod and R848 can not only enhance the migration of DCs but also induce the migration of human CD4<sup>+</sup> and CD8<sup>+</sup> T cells toward the topical treatment location [44,45]. As reported by Rosenberg et al., the TLR7/8 agonists might be an indispensable aid for T cells to destroy the established tumors [46]. Therefore, we further estimated the infiltration of T cells and cytotoxic T lymphocytes in tumor environment by immunohistochemical stainings for CD3 and CD8 in tumor sections in different treatment groups. The results are shown in Figs. 7E and S7. Obviously, the densities of intratumoral CD3<sup>+</sup> and CD8<sup>+</sup> T cells were sharply enhanced in treatment groups of free R848, DOX/R848 mixture, and HA-DOX/PHIS/R848 nanoparticles compared to both the control and free DOX-treated groups. This suggested that R848 could exert its regulation effect on the tumor immunity by promoting the infiltration of T cells and cytotoxic T lymphocytes into the tumor microenvironment. Moreover, the numbers of CD8<sup>+</sup> T cells in the treatment group of HA-DOX/PHIS/R848 nanoparticles were greater than those in the other treatment groups (Fig. S7), indicating that this therapeutic nanosystem triggered strong anti-tumor immune responses.

## 4. Conclusions

In this study, a dual pH-responsive multifunctional nanoparticle system was designed for targeted treatment of breast cancer by combining immunotherapy with chemotherapy. This nanoparticle system had a “core-shell” structure containing hydrophobic PHIS/R848 nanocore and hydrophilic HA-DOX shell, and realized the efficient release of R848 and DOX in orderly response to the acidic pHs of tumor microenvironment and endo/lysosomes. In immune cells, PHIS/R848 nanocores exhibited strong immunoregulatory activities similar to those induced by free R848. In breast cancer cells, HA-DOX was efficiently taken up by CD44-mediated internalization and significantly inhibited the cell proliferation. In 4T1 tumor-bearing mice, HA-DOX/PHIS/R848 nanoparticles showed excellent tumor-targeting ability due to the EPR and CD44-mediated active targeting effects and had remarkable synergistic effects on tumor growth by regulating tumor immunity and killing tumor cells. In conclusion, this multifunctional nanoparticle system showed great potential for clinical treatment of breast cancer by combining immunotherapy and chemotherapy.

## Acknowledgements

This work was supported by the National Natural Science Foundation of China (Grant Nos. 81602724, 81573005, and 81371671), the National High-tech R&D Program of China (863 Program 2015AA020403), the Tianjin 13th five year and TMU talent project (Grant No. 2016KJ0308), and the National Key Scientific Instrument and Equipment Development Project (2013YQ16055106). The authors gratefully thank Dr. De Yang (Frederick National Laboratory for Cancer Research, Maryland, USA) for his kind gift of DC2.4 and CAL-1 cell lines.

## Appendix A. Supplementary data

Supplementary data associated with this article can be found, in the online version, at <https://doi.org/10.1016/j.actbio.2017.11.010>.

## References

- [1] R.L. Siegel, K.D. Miller, A. Jemal, Cancer statistics, CA Cancer J. Clin. 66 (2016) 7–30.
- [2] D.F. Quail, J.A. Joyce, Microenvironmental regulation of tumor progression and metastasis, Nat. Med. 19 (2013) 1423–1437.
- [3] J.A. Kemp, M.S. Shim, C.Y. Heo, Y.J. Kwon, "Combo" nanomedicine: Co-delivery of multi-modal therapeutics for efficient, targeted, and safe cancer therapy, Adv. Drug Deliv. Rev. 98 (2016) 3–18.
- [4] P. Gotwals, S. Cameron, D. Cipolletta, V. Cremasco, A. Crystal, B. Hewes, S. Quarantino, C. Sabatos-Peyton, L. Petruzzelli, J.A. Engelmann, G. Dranoff, Prospects for combining targeted and conventional cancer therapy with immunotherapy, Nat. Rev. Cancer 17 (2017) 286–301.
- [5] D. Peer, J.M. Karp, S. Hong, O.C. Farokhzad, R. Margalit, R. Langer, Nanocarriers as an emerging platform for cancer therapy, Nat. Nanotechnol. 2 (2007) 751–760.
- [6] T. Sun, Y.S. Zhang, B. Pang, D.C. Hyun, M. Yang, Y. Xia, Engineered nanoparticles for drug delivery in cancer therapy, Angew. Chem. Int. Ed. 53 (2014) 12320–12364.
- [7] S. Mura, J. Nicolas, P. Couvreur, Stimuli-responsive nanocarriers for drug delivery, Nat. Mater. 12 (2013) 991–1003.
- [8] A.S. Hoffman, Stimuli-responsive polymers: biomedical applications and challenges for clinical translation, Adv. Drug Deliv. Rev. 65 (2013) 10–16.
- [9] C. He, J. Lu, W. Lin, Hybrid nanoparticles for combination therapy of cancer, J. Control Release 219 (2015) 224–236.
- [10] J.R. Brahmer, S.S. Tykodi, L.Q. Chow, W.J. Hwu, S.L. Topalian, P. Hwu, C.G. Drake, L.H. Camacho, J. Kauh, K. Odunsi, H.C. Pitot, O. Hamid, S. Bhatia, R. Martins, K. Eaton, S. Chen, T.M. Salay, S. Alaparthi, J.F. Gross, A.J. Korman, S.M. Parker, S. Agrawal, S.M. Goldberg, D.M. Pardoll, A. Gupta, J.M. Wigginton, Safety and activity of anti-PD-L1 antibody in patients with advanced cancer, N. Engl. J. Med. 366 (2012) 2455–2465.
- [11] E.B. Garon, N.A. Rizvi, R. Hui, N. Leighl, A.S. Balmanoukian, J.P. Eder, A. Patnaik, C. Aggarwal, M. Gubens, L. Horn, E. Carcereny, M.J. Ahn, E. Felip, J.S. Lee, M.D. Hellmann, O. Hamid, J.W. Goldman, J.C. Soria, M. Dolled-Filhart, R.Z. Rutledge, J. Zhang, J.K. Lunceford, R. Rangwala, G.M. Lubiniecki, C. Roach, K. Emancipator, L. Gandhi, Pembrolizumab for the treatment of non-small-cell lung cancer, N. Engl. J. Med. 372 (2015) 2018–2028.
- [12] I. Akiko, M. Ruslan, Control of adaptive immunity by the innate immune system, Nat. Immunol. 16 (2015) 343–353.
- [13] T. Kawai, S. Akira, Toll-like receptors and their crosstalk with other innate receptors in infection and immunity, Immunity 34 (2011) 637–650.
- [14] E. Vacchelli, L. Galluzzi, A. Eggermont, W.H. Fridman, J. Galon, C. Sautès-Fridman, E. Tartour, L. Zitvogel, G. Kroemer, Trial watch: FDA-approved Toll-like receptor agonists for cancer therapy, Oncoimmunology 1 (2012) 894–907.
- [15] M.P. Schön, M. Schön, TLR7 and TLR8 as targets in cancer therapy, Oncogene 27 (2008) 190–199.
- [16] M. Jurk, F. Heil, J. Vollmer, C. Schetter, A.M. Krieg, H. Wagner, G. Lipford, S. Bauer, Human TLR7 or TLR8 independently confer responsiveness to the antiviral compound R-848, Nat. Immunol. 3 (2002) 499.
- [17] X. Wu, Y. Wu, H. Ye, S. Yu, C. He, X. Chen, Interleukin-15 and cisplatin co-encapsulated thermosensitive poly(peptide hydrogels for combined immuno-chemotherapy, J. Control Release 255 (2017) 81–93.
- [18] A. Seth, M.B. Heo, Y.T. Lim, Poly( $\gamma$ -glutamic acid) based combination of water-insoluble paclitaxel and TLR7 agonist for chemo-immunotherapy, Biomaterials 35 (2014) 7992–8001.
- [19] E.S. Lee, K. Na, Y.H. Bae, Super pH-sensitive multifunctional polymeric micelle, Nano Lett. 5 (2005) 325–329.
- [20] R.A. Cardone, V. Casavola, S.J. Reshkin, The role of disturbed pH dynamics and the Na<sup>+</sup>/H<sup>+</sup> exchanger in metastasis, Nat. Rev. Cancer 5 (2005) 786–795.
- [21] E.S. Lee, K.T. Oh, D. Kim, Y.S. Youn, Y.H. Bae, Tumor pH-responsive flower-like micelles of poly(L-lactic acid)-b-poly(ethylene glycol)-b-poly(L-histidine), J. Control Release 123 (2007) 19–26.
- [22] K.T. Dicker, L.A. Gurski, S. Pradhan-Bhatt, R.L. Witt, M.C. Farach-Carson, X. Jia, Hyaluronan: a simple polysaccharide with diverse biological functions, Acta Biomater. 10 (2014) 1558–1570.
- [23] C. Yang, X. Wang, X. Yao, Y. Zhang, W. Wu, X. Jiang, Hyaluronic acid nanogels with enzyme-sensitive cross-linking group for drug delivery, J. Control Release 205 (2015) 206–217.
- [24] G. Mattheolabakis, L. Milane, A. Singh, M.M. Amiji, Hyaluronic acid targeting of CD44 for cancer therapy: from receptor biology to nanomedicine, J. Drug Target 23 (2015) 605–618.
- [25] X. Deng, M. Cao, J. Zhang, K. Hu, Z. Yin, Z. Zhou, X. Xiao, Y. Yang, W. Sheng, Y. Wu, Y. Zeng, Hyaluronic acid-chitosan nanoparticles for co-delivery of MiR-34a and doxorubicin in therapy against triple negative breast cancer, Biomaterials 35 (2014) 4333–4344.
- [26] M. Karimi, A. Ghazemi, P. Sahandi Zangabad, R. Rahighi, S.M. Moosavi Basri, H. Mirshekari, M. Amiri, Z. Shafaei Pishabad, A. Aslani, M. Bozorgomid, D. Ghosh, A. Beyzavi, A. Vaseghi, A.R. Aref, L. Haghani, S. Bahrami, M.R. Hamblin, Smart micro/nanoparticles in stimulus-responsive drug/gene delivery systems, Chem. Soc. Rev. 45 (2016) 1457–1501.
- [27] S. Cai, S. Thati, T.R. Bagby, H.M. Diab, N.M. Davies, M.S. Cohen, M.L. Forrest, Localized doxorubicin chemotherapy with a biopolymeric nanocarrier improves survival and reduces toxicity in xenografts of human breast cancer, J. Control Release 146 (2010) 212–218.
- [28] Y. Wang, G. Wan, Z. Li, S. Shi, B. Chen, C. Li, L. Zhang, Y. Wang, PEGylated doxorubicin nanoparticles mediated by HN-1 peptide for targeted treatment of oral squamous cell carcinoma, Int. J. Pharm. 525 (2017) 21–31.
- [29] C. Fu, H. Li, N. Li, X. Miao, M. Xie, W. Du, L.M. Zhang, Conjugating an anticancer drug onto thiolated hyaluronic acid by acid labile hydrazone linkage for its gelation and dual stimuli-response release, Carbohydr. Polym. 128 (2015) 163–170.
- [30] E.S. Lee, H.J. Shin, K. Na, Y.H. Bae, Poly(L-histidine)-PEG block copolymer micelles and pH-induced destabilization, J. Control Release 90 (2003) 363–374.
- [31] J. Liu, Y. Huang, A. Kumar, A. Tan, S. Jin, A. Mozhi, X.J. Liang, pH-sensitive nanosystems for drug delivery in cancer therapy, Biotechnol. Adv. 32 (2014) 693–710.
- [32] Y. Liu, W. Wang, J. Yang, C. Zhou, J. Sun, pH-sensitive polymeric micelles triggered drug release for extracellular and intracellular drug targeting delivery, Asian J. Pharm. Sci. 8 (2013) 159–167.
- [33] I. Mellman, R.M. Steinman, Dendritic cells: specialized and regulated antigen processing machines, Cell 106 (2001) 255–258.
- [34] T. Maeda, K. Murata, T. Fukushima, K. Sugahara, K. Tsuruda, M. Anami, Y. Onimaru, K. Tsukasaki, M. Tomonaga, R. Moriuchi, H. Hasegawa, Y. Yamada, S. Kamihira, A Novel plasmacytoid dendritic cell line, CAL-1, established from a patient with blastic natural killer cell lymphoma, Int. J. Hematol. 81 (2005) 148–154.
- [35] F. Steinhaugen, A.P. McFarland, L.G. Rodriguez, P. Tewary, A. Jarret, R. Savan, D. M. Klinman, IRF-5 and NF-kappaB p50 co-regulate IFN-beta and IL-6 expression in TLR9-stimulated human plasmacytoid dendritic cells, Eur. J. Immunol. 43 (2013) 1896–1906.
- [36] C. Reis e Sousa, Activation of dendritic cells: translating innate into adaptive immunity, Curr. Opin. Immunol. 16 (2004) 21–25.
- [37] J.M. Wickens, H.O. Alsab, P. Kesharwani, K. Bhise, M.C.I.M. Amin, R.K. Tekade, U. Gupta, A.K. Iyer, Recent advances in hyaluronic acid-decorated nanocarriers for targeted cancer therapy, Drug Discov. Today 22 (2017) 665–680.
- [38] M. Li, Z. Tang, D. Zhang, H. Sun, H. Liu, Y. Zhang, Y. Zhang, X. Chen, Doxorubicin-loaded polysaccharide nanoparticles suppress the growth of murine colorectal carcinoma and inhibit the metastasis of murine mammary carcinoma in rodent models, Biomaterials 51 (2015) 161–172.
- [39] F. Li, W.L. Chen, B.G. You, Y. Liu, S.D. Yang, Z.Q. Yuan, W.J. Zhu, J.Z. Li, C.X. Qu, Y. J. Zhou, X.F. Zhou, C. Liu, X.N. Zhang, Enhanced cellular internalization and on-demand intracellular release of doxorubicin by stepwise pH-reduction-responsive nanoparticles, ACS Appl. Mater. Interfaces 8 (2016) 32146–32158.
- [40] F. Kuonen, J. Laurent, C. Secondini, G. Lorusso, J.C. Stehle, T. Rausch, E. Faes-Van't Hull, G. Bieler, G.C. Alghisi, R. Schwendener, S. Andrejevic-Blant, R.O. Mirimanoff, C. Rueegg, Inhibition of the Kit ligand/c-Kit axis attenuates metastasis in a mouse model mimicking local breast cancer relapse after radiotherapy, Clin. Cancer Res. 18 (2012) 4365–4374.
- [41] S.J. Dovedi, M.H. Melis, R.W. Wilkinson, A.L. Adlard, I.J. Stratford, J. Honeychurch, T.M. Illidge, Systemic delivery of a TLR7 agonist in combination with radiation primes durable antitumor immune responses in mouse models of lymphoma, Blood 121 (2013) 251–259.
- [42] D. Wang, M. Precopio, T. Lan, D. Yu, J.X. Tang, E.R. Kandimalla, S. Agrawal, Antitumor activity and immune response induction of a dual agonist of Toll-like receptors 7 and 8, Mol. Cancer Ther. 9 (2010) 1788–1797.
- [43] A. Contreras, S. Sen, A.J. Tatar, D.A. Mahvi, J.V. Meyers, P. Srinand, S. Agrawal, M. Suresh, C.S. Cho, Enhanced local and systemic anti-melanoma CD8+ T cell responses after memory T cell-based adoptive immunotherapy in mice, Cancer Immunol. Immunother. 65 (2016) 601–611.
- [44] M.P. Schon, M. Schon, TLR7 and TLR8 as targets in cancer therapy, Oncogene 27 (2008) 190–199.
- [45] T. Yin, S. He, Y. Wang, Toll-like receptor 7/8 agonist, R848, exhibits antitumoral effects in a breast cancer model, Mol. Med. Rep. 12 (2015) 3515–3520.
- [46] E. Tran, P.F. Robbins, S.A. Rosenberg, 'Final common pathway' of human cancer immunotherapy: targeting random somatic mutations, Nat. Immunol. 18 (2017) 255–262.